FORMULATION OF CALCIUM-CROSSLINKED ZEIN-GELLAN GUM NANOPARTICLES FOR NARINGENIN DELIVERY: STABILITY, DIGESTION SIMULATION, AND ANTIOXIDANT EVALUATION

SHIVAJI JADHAV,[*] SOPAN NANGARE,[**] PIYUSH BAFNA,[***] PREMKUMAR BAVISKAR[*] and LAXMIKANT ZAWAR[*]

[*]*Department of Pharmaceutics, H. R. Patel Institute of Pharmaceutical Education and Research, Shirpur 425405, Maharashtra State, India*

[**] *Department of Pharmaceutics, Krishna Institute of Pharmacy, Krishna Vishwa Vidyapeeth (Deemed to be University), Karad 415539, Maharashtra State, India*

[***]*Department of Pharmacology, H. R. Patel Institute of Pharmaceutical Education and Research, Shirpur 425405, Maharashtra State, India*

✉ *Corresponding author: L. R. Zawar, shwet.zawar@gmail.com*

Received March 20, 2025

Naringenin (NR), a bioactive flavonoid with antioxidant and therapeutic potential, has limited pharmaceutical and nutraceutical applications owing to its poor water solubility and stability. To overcome these challenges, this study presents a novel core-shell nanocarrier system comprising zein (Zn) nanoparticles coated with calcium-crosslinked gellan gum (GG) for enhanced NR stability and sustained release. Zn-NR-GG nanoparticles were formulated via anti-solvent precipitation and calcium-mediated gelation, resulting in a uniform gel network with an average size of 234 nm. The GG shell provides structural integrity, preventing nanoparticle aggregation and enzymatic degradation under simulated gastrointestinal conditions. The nanoparticles exhibited high encapsulation efficiency (>91%), enhanced antioxidant activity, and a controlled NR release profile of 56.66 ± 0.11% over 4 h. The stability assessments demonstrated resistance to thermal, ionic, and pH variations, underscoring their robustness for bioactive delivery. The integration of protein-polysaccharide interactions with calcium-induced gelation offers an effective strategy for improving NR solubility, bioavailability, and therapeutic efficacy. This study highlights Zn-NR-GG nanoparticles as promising polymeric biomaterials for controlled nutraceutical and pharmaceutical applications.

Keywords: zein, naringenin, gellan gum, calcium-induced gelation, core–shell nanoparticles, antioxidant study

INTRODUCTION

Naringenin (NR) is a flavonoid commonly found in citrus fruits, including oranges, grapefruits, lemons, tomatoes, tangerines, and other edible fruits.[1] Research has demonstrated that NR offers various physiological effects, including antihypertensive,[2] anti-inflammatory,[3] anti-cancer,[4,5] anti-obesity,[6] and antioxidant[7,8] properties. Despite these advantages, the practical application of NR is considerably constrained by its poor water solubility. Hence, it limits the utilization of NR in nutraceuticals and pharmaceutical applications.[9] Various strategies have been investigated to overcome these limitations. Nanotechnology has emerged as a promising solution.[10,11] Proteins and polysaccharides are natural polymers with structure-forming characteristics, making them ideal for creating a nano-enabled technique for NR. Among these strategies, protein-based nanoparticles, particularly those composed of zein (Zn), have garnered substantial attention owing to their safety and efficacy.[12]

Zn is the primary storage protein in maize. Moreover, Zn is a biocompatible and biodegradable plant protein approved by the FDA. It displays distinctive amphiphilic properties owing to its high levels of nonpolar amino acids, such as alanine, leucine, and proline, coupled with a low concentration of polar amino acids. This property facilitates Zn dissolution in 55–95% ethanol and highly alkaline solutions (pH > 11). Consequently, Zn can self-assemble into

nanoparticles using an anti-solvent precipitation method. To address this, Zn nanoparticles have been successfully used to deliver 5-fluorouracil, leveraging Zn's biodegradable and amphiphilic properties.[13] However, Zn nanoparticles tend to aggregate around their isoelectric point and exhibit limited encapsulation efficiency and loading capacity, as well as limited opposition to heat, salts, acids, bases, and oxidation.[13,14] These issues can be addressed by coating Zn nanoparticles with hydrophilic polysaccharides, which prevents aggregation and enhances stability, encapsulation efficiency, and loading capacity.[15,16] Therefore, there is a need to coat Zn nanoparticles with an appropriate coating agent that can overcome these limitations.

Several studies have explored the formation, stability, and functionality of polysaccharide-coated Zn nanoparticles. These nanoparticles have been coated with a range of polysaccharides, such as chitosan,[17] carboxymethyl dextrin[18] and *Mesona chinensis* polysaccharide.[19] In these systems, Zn serves as the "core" that houses hydrophobic compounds (drugs), while the polysaccharide shell attaches to the core through electrostatic interactions.[20] Hence, we intended to use the polysaccharide shell and design a core-shell nanoparticle system for drug delivery applications.

Gellan gum (GG) is derived from the bacterium *Pseudomonas elodea*. It is an anionic heteropolysaccharide that is known for its biocompatibility, biodegradability, and hydrogel-forming ability. It consists of repeating units of *α-L*-rhamnose, *β-D*-glucuronic acid, and *β*-D-glucose.[21] It has also been authorized by the FDA and the European Community for use as a stabilizer, thickener, and gelling agent.[22] GG gels offer protection to bioactive substances from the acidic conditions of the stomach, thereby enhancing their stability and effectiveness. These gels gradually dissolve in alkaline environments, suggesting the potential of GG to regulate the release of encapsulated compounds within the gastrointestinal tract.[23,24]

Unfortunately, the ionic linkages in Zn and natural polysaccharides may become unstable in the gastrointestinal tract (GIT) owing to pH fluctuations and the strength of electrostatic interactions.[20] Therefore, it is crucial to enhance the interaction between Zn and polysaccharides with crosslinkers. There is a need to design an advanced approach that can induce polysaccharide gelation and form nanogels with a more resilient "shell". Calcium ions can act as stabilizing cross-linkers, creating a polysaccharide gel network around Zn nanoparticles and enhancing their stability and efficacy.[25] Importantly, GG can form gels in the presence of cations, such as calcium, enhancing its stability and making it suitable for food and pharmaceutical applications.[26] Therefore, the present work aimed to design Zn nanoparticles coated with GG using a Ca^{2+} crosslinker.

In this study, we designed NR encapsulated Zn nanoparticles coated with GG (Zn-NR-GG) using a calcium (Ca^{2+}) crosslinker. Core Zn-NR nanoparticles were synthesized using the anti-solvent precipitation method and then coated with GG through calcium-mediated gelation, which formed a protective shell. This formulation enabled the controlled release of NR from the Zn-GG nanogel system during *in vitro* digestion. Additionally, the physical stability of the nanoparticles, including pH tolerance, resistance to ionic strength fluctuations, and thermal resilience, were demonstrated to be robust. The antioxidant capacity of the encapsulated NR was enhanced by the synergistic effects of the formulation. Therefore, this work presents a novel solution for encapsulating, stabilizing, and controlling the release of NR using Zn-GG nanoparticles. In the future, this GG-coated Zn core-shell system could have significant applications in the nutraceutical and pharmaceutical fields.

EXPERIMENTAL

Materials

Low-acyl gellan gum (KELCOGEL® CG-LA) was purchased from CP Kelco Mumbai, India. Zein (Zn, MW: 25-40 kDa) was obtained from TCI Chemical, Pvt. Ltd., India. Naringenin (99%) and bile salts were supplied by the Sisco Research Lab. Pvt. Ltd., Mumbai, India. Pepsin 1:3000 and pancreatin were procured from Loba Chemie Pvt. Ltd. Mumbai, India.

Methods

Preparation of Zn-NR-GG nanoparticles

First, Zn-NR nanoparticles were synthesized using an anti-solvent precipitation method.[27] Initially, 0.9 g of Zn and 0.3 g of NR were dissolved in an 80% ethanol-water solution (100 mL, v/v). The resulting mixture was magnetically stirred at 600 rpm for 30 min. It was then added dropwise to 300 mL of deionized water at pH 4.0, with continuous stirring for 1 h to form Zn-NR nanoparticles. Subsequently, ethanol was removed from the Zn–NR nanoparticle dispersion using a rotary evaporator at 40 °C, and the

volume was adjusted to 100 mL with deionized water to obtain a stable aqueous suspension.

In the next step, several Zn/GG mass ratios, such as 10:1, 5:1, 2:1, 1:1 and 1:2 (m/m), denoted as Zn-NR-GG (10:1), Zn-NR-GG (5:1), Zn-NR-GG (2:1), Zn-NR-GG (1:1), and Zn-NR-GG (1:2), were used. The prepared Zn-NR nanoparticles were then added dropwise into a GG solution (0.09–1.8% w/v) at pH 4 in equal volumes, while stirring at 300 rpm on a magnetic stirrer to form Zn-NR-GG nanoparticles. Calcium (Ca^{2+}) crosslinking of the Zn-NR-GG nanoparticles was achieved by adding a 5 mmol/L $CaCl_2$ solution with continuous stirring to form gelation of the GG layer.

After nanoparticle formation, the dispersion was centrifuged at 12,000 rpm for 20 min at 4 °C to pellet the nanoparticles. The supernatant containing unencapsulated NR, excess GG, and free Ca^{2+} ions was discarded. The nanoparticle pellet was washed twice with deionized water and resuspended to obtain a purified nanoparticle suspension. The purified nanoparticle suspension was divided into two portions: one portion was stored at 4 °C in a refrigerator, and the other portion was subjected to freeze-drying to obtain dry powders. The resulting freeze-dried samples were gently ground using a mortar and pestle, and stored in a desiccator until further use. These powders were used directly for solid-state characterization.

Characterization of nanoparticles: spectral analysis

Powder X-ray diffraction (PXRD) was performed using a wide-angle X-ray diffractometer (Bruker D8, Germany). In short, the instrument utilized Cu-Kα radiation (λ = 0.15418 nm) generated by a copper anode with an operating voltage of 40 keV and a current of 40 mA. The diffractograms of the samples were obtained by continuous scanning at a rate of 5°/min over a 0–50° range of 2θ.

Particle size, polydispersity index (PDI), and zeta potential were analyzed using a Nanoplus3 instrument (Particle Size and Zeta Analyzer, Micromeritics, USA) at 25 °C with a scattering angle of 90°. The surface characteristics of the nanoparticles were analyzed using scanning electron microscopy (SEM, JEOL, JSM-6390 LV USA). Fourier transform infrared spectroscopy (FTIR, Bruker Vertex 70, Alpha-II) was utilized to investigate the chemical composition and molecular interactions within nanoparticles containing NR, GG, Zn, Zn-NR, and Zn-NR-GG nanoparticles. The samples were positioned on the detector and scanned at 25 °C, with resolutions ranging from 400 to 4000 cm^{-1}. The thermal analysis of NR, Zn, GG, Zn-NR, and Zn-NR-GG nanoparticles was investigated using differential scanning calorimetry (DSC, TA Instruments, USA). Briefly, the samples were placed in aluminum sample pans and subjected to a temperature ramp of 10 °C/min from 50 °C to 280 °C. Fluorescence analysis was performed using a spectrofluorometer (JASCO International Co. Ltd., Tokyo, Japan) at 25 °C. Before analysis, the pH of the nanoparticle suspensions was adjusted to 3.5 by dilution with water, resulting in a solution containing 0.2 mg/mL of Zn. The excitation wavelength was fixed at 280 nm and the emission spectra were recorded in the range of 290–450 nm.

Loading capacity (LC) and encapsulation efficiency (EE)

In this step, the NR encapsulation and loading capacity within the Zn-NR-GG nanoparticles were evaluated.[28] Briefly, freshly prepared samples were centrifuged at 8000 rpm for 30 min, followed by dilution with an 80% ethanol aqueous solution to achieve the desired concentration. The absorbance of the resulting solution at 288 nm was measured using UV–Vis spectroscopy. During UV-Vis spectrophotometric measurements at 288 nm, corresponding Zn blank solutions (prepared under identical conditions, without NR) were used as references to correct for any background absorbance. At last, the NR concentration in Zn-NR-GG nanoparticles was determined as LC (%) and EE (%) using the following formulas:

$$\text{EE (\%)} = \frac{\text{Total NR mass (mg)} - \text{free NR mass (mg)}}{\text{Total NR mass (mg)}} \times 100 \quad (1)$$

$$\text{LC (\%)} = \frac{\text{Total NR mass (mg)} - \text{free NR mass (mg)}}{\text{Total mass of nanoparticles}} \times 100 \quad (2)$$

Antioxidant activity

In this study, the antioxidant activities of both free NR and nanoparticles were evaluated using a DPPH radical scavenging assay.[6] Briefly, a 4 mL aliquot of a 0.1 mM DPPH-ethanol solution was mixed with 4 mL of bulk NR and nanoparticles (Zn-NR and Zn-NR-GG) with continuous stirring at 50 rpm for 5 min. For the nanoparticle samples, the amount of Zn-NR or Zn-NR-GG added was adjusted based on the measured NR loading to ensure that the final NR concentration in all samples was identical. The resulting mixture was incubated at room temperature in the dark for 30 min. The absorbance of each sample was measured at 517 nm using a UV-Vis spectrophotometer. Finally, the radical scavenging activity was calculated using Equation (3):

$$\text{RS (\%)} = \frac{\text{Abs.of DPPH} - \text{Abs.of sample}}{\text{Abs.of DPPH}} \times 100 \quad (3)$$

Stability evaluation

Stability experiments were performed on the Zn-NR and Zn-NR-GG nanoparticles, including changes in pH, temperature fluctuations, variations in ionic strength, and storage duration. Briefly, 10 mL of freshly prepared Zn-NR and Zn-NR-GG nanoparticles (n = 3) were incubated at 40, 50, 60, 70, 80, and 90 °C for 45 min in a water bath. After heating, the nanoparticles were cooled to room temperature for further analysis. The obtained nanoparticle samples were then subjected to zeta potential and particle size analyses. Similarly, freshly prepared 10 mL of Zn-NR

and Zn-NR-GG nanoparticles were subjected to continuous mixing for 20 min at different NaCl concentrations (10, 20, 50, 100, and 200 mmol/L). The obtained nanoparticle samples were then subjected to zeta potential and particle size analyses. After this study, the pH stability of the formulated nanoparticles was evaluated. Freshly prepared 10 mL of Zn-NR and Zn-NR-GG nanoparticles were adjusted to pH values ranging from 4 to 8 using 0.1 M NaOH and 0.1 M HCl solutions. The suspensions were allowed to equilibrate for 10 min before assessment. The obtained nanoparticle samples were then subjected to zeta potential and particle size analyses. Finally, freshly prepared Zn-NR and Zn-NR-GG nanoparticles were stored at 4 °C. The samples were evaluated weekly at room temperature (25 °C). The obtained nanoparticle samples were then subjected to zeta potential and particle size analysis to ensure stability for a longer duration.

In vitro *simulated gastrointestinal digestion*

In vitro simulated gastrointestinal digestion of the prepared nanoparticles was conducted using the dialysis membrane technique.[29] In short, Zn-NR, Zn-NR-GG, NR-GG, and bulk NR dispersion in deionized water were incorporated into the dialysis bags, separately and sealed to avoid the leakage of nanoparticles in dissolution media. The sealed dialysis bags were then placed in a flask containing 150 mL of simulated gastric fluid (SGF). SGF was prepared by adding 2 mg/mL NaCl and 3.2 mg/mL pepsin, adjusting the pH to 1.2 with 1 M HCl, and agitating at 37 °C for 1 h. Following gastric digestion, the dialysis bags were sealed and transferred to 150 mL of simulated intestinal fluid (SIF) at pH 6.8. SIF was prepared by adjusting the pH with 1 M HCl and including 8.8 mg/mL NaCl, 6.8 mg/mL KH_2PO_4, and 2.0 mg/mL bile salts. During digestion, 5 mL samples were collected at 30, 60, 90, 120, 150, 180, 210, and 240 min, and sink conditions were maintained by replacing the withdrawn volume with fresh buffer. The amount of NR released at each interval was determined using calibration curves prepared in SGF and SIF. Briefly, standard NR solutions in SGF and SIF (2–12 ppm) were measured at 288 nm to generate linear calibration curves ($R^2 > 0.995$), which were subsequently used for quantification of NR released from the nanoparticles (Eq. 4).

$$\text{Digestive release rate (\%)} = \frac{\text{Wt .of released NR (mg)}}{\text{Wt.of NR before digestion (mg)}} \times 100 \quad (4)$$

Statistical analysis

Each experiment was performed in triplicate, and the results are presented as mean ± standard deviation (SD). Statistical significance was set at $p < 0.05$. Statistical analyses, including one-way analysis of variance (ANOVA), were used to identify significant differences between the experimental groups.

RESULTS AND DISCUSSION

Particle size, polydispersity index, and zeta potential analysis

Figure 1A illustrates the particle size and PDI of Zn, Zn-NR, and Zn-NR-GG nanoparticles. In short, the Zn nanoparticles exhibited an average size of 161.5 nm (PDI: 0.19), which was larger compared to the Zn-NR nanoparticles with an average size of 97.2 nm (PDI: 0.14). The decrease in size upon NR loading is likely due to hydrophobic interactions between NR and the hydrophobic domains of Zn, which may promote a more compact particle structure during the anti-solvent precipitation process.[30] In contrast to Zn and Zn-NR nanoparticles, Zn-NR-GG nanoparticles showed significantly larger sizes, with mean diameters increasing from approximately 234 nm to 500 nm as the concentration of GG was increased from 0.18 g to 1.8 g. Here, the size increased, which might be due to electrostatic interactions between positively charged regions on the surfaces of Zn nanoparticles and anionic regions on GG molecules. This led to the formation of a polysaccharide-based shell that increased the overall particle size.[3] Additionally, polysaccharides facilitate nanoparticle aggregation through a bridging mechanism, further contributing to size increase.[6,30] The pronounced size increase observed for Zn-NR-GG (1:2) particles ($p < 0.05$) may be attributed to ionic cross-linking of GG molecules by Ca^{2+} ions.[31]

Initially, at low GG concentrations (higher Zn ratios such as 10:1), the GG molecules are insufficient to cause significant variation in particle size, resulting in a relatively low PDI of 0.19. As the GG concentration increased to an optimal ratio (5:1), the interaction between GG and Zn was balanced. This led to a uniform particle size distribution, reflected by a PDI of 0.25. The optimal uniformity suggests that the GG molecules were adequately dispersed and interacted uniformly with Zn. However, as the GG concentration continued to increase beyond this optimal point (ratios of 2:1, 1:1, and 1:2), the interactions between GG and Zn became more complex. Higher GG concentrations led to enhanced electrostatic interactions and aggregation, resulting in increased particle size heterogeneity. The increased heterogeneity was due to the formation of larger aggregates and variable particle structures, as indicated by higher PDI values of 0.28, 0.29, and 0.30 at these ratios.

Excessive GG molecules may also promote bridging flocculation, where GG chains link multiple Zn particles together, further contributing to size variability.[30]

The zeta potential of Zn nanoparticles was found to be +11.0 mV, whereas Zn-NR nanoparticles demonstrated a +12.48 mV zeta potential (Fig. 1B). This positive charge arises because the pH is below the isoelectric point of Zn. In contrast, Zn nanoparticles coated with GG and crosslinked with Ca^{2+} displayed a negative charge of -15.0 mV to -26.0 mV. The negative charge was attributed to the anionic glucuronic acid content in the GG coating. Moreover, as the concentration of GG increased, the zeta potential of Zn-NR-GG nanoparticles became more negative, indicating more effective coverage of the Zn nanoparticles by anionic polysaccharides.[32]

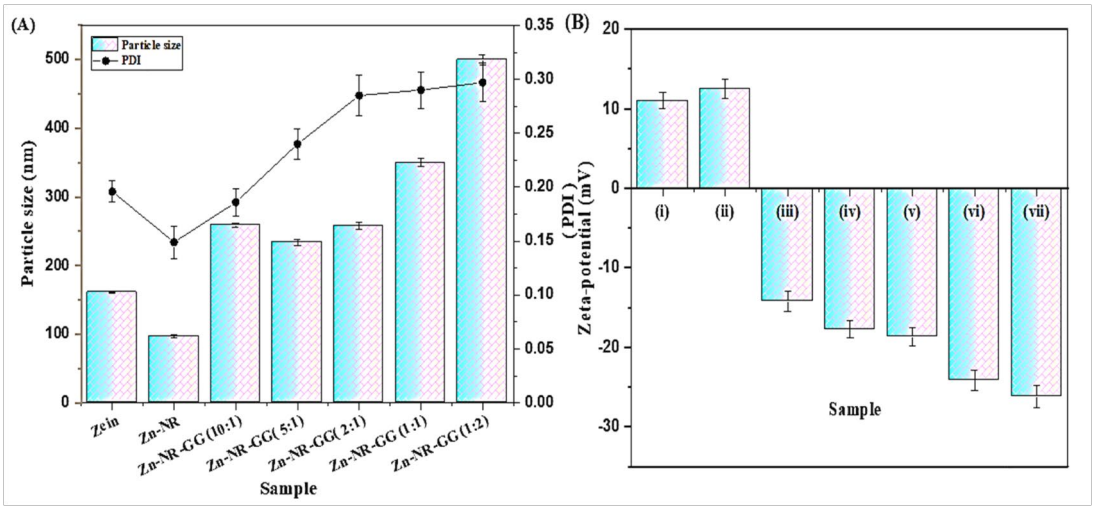

Figure 1: (A) Measurement of particle size and PDI, (B) Zeta-potential of (i) Zn, (ii) Zn-NR, (iii) Zn-NR-GG (10:1), (iv) Zn-NR-GG (5:1), (v) Zn-NR-GG (2:1), (vi) Zn-NR-GG (1:1), (vii) Zn-NR-GG (1:2) nanoparticles

Loading capacity and encapsulation efficiency

Figure 2A presents the results for %EE and %LC of the NR in the Zn-NR and Zn-NR-GG nanoparticles. Here, the %EE for Zn-NR nanoparticles was measured to be 77.58 ± 0.17%. However, upon coating with GG, the %EE for Zn-NR-GG (10:1) nanoparticles significantly increased to 91.05 ± 0.07%, indicating that GG enhanced NR encapsulation within the Zn nanoparticles. When the ratio of Zn to GG reached 5:1, the EE further increased to 92.32 ± 0.42%, suggesting that a thicker GG coating provided a more effective barrier against NR leakage. This was corroborated by the practical increase in the particle size of the Zn-NR-GG nanoparticles. The higher encapsulation efficiency of NR in Zn-NR-GG nanoparticles, compared with Zn-NR, can be attributed to the presence of the GG shell, which effectively limits the leakage of naringenin from the zein core. Similar observations have been reported for curcumin-loaded zein nanoparticles coated with ι-carrageenan, where the formation of a thicker polysaccharide coating reduced bioactive leakage and increased particle size, confirming successful core–shell formation. This suggests that the GG layer acts as a physical barrier, enhancing the retention of NR within the nanoparticles.[30]

The %EE for Zn-NR-GG nanoparticles remained statistically unchanged ($p > 0.05$) when the ratio varied from 2:1 to 1:2, likely due to the robust nature of the GG coating, effectively preventing NR leakage. The %LC for both Zn-NR and Zn-NR-GG nanoparticles was 22.2 ± 0.032%. However, as the mass ratio of Zn to GG increased from 10:1 to 1:2, %LC decreased. This decrease in %LC was attributed to the substantial increase in the overall weight of the core-shell nanoparticles, despite the increasing quantity of NR in the core-shell structure with increasing GG concentration.[33] Overall, these findings indicate that the interaction between negatively charged GG molecules and positively charged Zn nanoparticles resulted in the formation of polysaccharide-coated protein nanoparticles. Hence, it improved the NR encapsulation. The incorporation of Ca^{2+} to crosslink the GG molecules in the coating further minimizes NR

leakage. This combination of GG complexation and Ca^{2+} ion crosslinking significantly improves both the %EE and %LC of NR. The optimized Zn-NR-GG nanoparticles were formulated at a mass ratio of 5:1 (Zn:GG) based on particle size, PDI, zeta potential, encapsulation efficiency, and loading capacity.

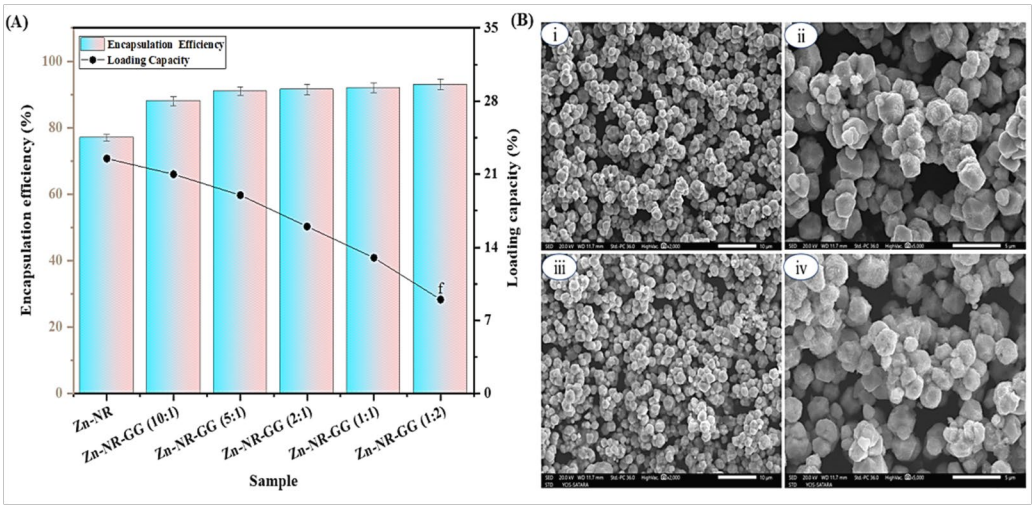

Figure 2: Loading capacity and encapsulation efficiency (A) and SEM (B) of Zn-NR (i, ii) and Zn-NR-GG (iii, iv) nanoparticles

SEM

In this step, SEM analysis was employed to examine the Zn-NR and Zn-NR-GG nanoparticles after freeze-drying (Fig. 2B). Herein, the Zn-NR dispersions displayed small, spherical nanoparticles with well-defined boundaries and uniform dimensions, which was attributed to the self-assembly capability of Zn during the anti-solvent precipitation process.[34] The Zn-NR-GG nanoparticles maintained their spherical shape, but were larger compared to the Zn-NR nanoparticles. The size of the final nanoparticles (5:1) increased, which might be due to the polysaccharide coating formed around the protein nanoparticles. The surface texture of the Zn-NR-GG nanoparticles was rough, forming a three-dimensional network-like structure. This roughness and network formation are due to the cross-linking of GG molecules via hydrogen bonding among –OH, and –COOH groups, as well as additional crosslinking facilitated by Ca^{2+} ions. Overall, these results imply that Zn-NR-GG dispersions function as microgels, effectively entrapping Zn nanoparticles.[35,36]

DSC analysis

The thermogram of NR exhibits a distinct endothermic peak at approximately 253°, indicating its crystalline nature (Fig. 3A).[37] The thermogram of Zn and GG does not display any characteristic peaks ensuring the amorphous nature. Notably, the thermogram of Zn-NR and Zn-NR-GG nanoparticles ensured the disappearance of the NR endothermic peak. This disappearance suggests that NR adopts an amorphous form when encapsulated within nanoparticles.[38] The thermal stability of Zn nanoparticles makes them suitable for encapsulating heat-sensitive materials. The enhanced thermal stability is likely due to the presence of hydrophobic groups and sulfhydryl (SH) content in the Zn protein. Additionally, changes in the secondary structure of Zn during nanoparticle formation may reinforce the hydrophobic interactions, hydrogen bonds, and electrostatic attractions between the Zn core and the GG shell. The formation of these nanoparticles might be largely driven by the hydrophobic interaction between Zn and NR. Encapsulating NR within a Zn-GG matrix provides effective thermal protection, even in harsh environments. This encapsulation strategy not only stabilizes NR, but also enhances the applicability of Zn nanoparticles for delivering heat-sensitive compounds.

PXRD

Figure 3B reveals that the NR exhibits characteristic high-intensity peaks at 2θ = 10.92°, 15.89°, 17.34°, 18.18°, 20.04°, 20.53°, 21.45°, 22.43°, 23.90°, 24.57°, 25.52°, 25.95°, and 27.82°. This confirms the crystalline nature of

NR. In contrast, the diffractogram of powdered Zn displays peaks at 2θ = 9.7° and 19.5°, while powdered GG showed a single broad peak at 2θ = 20.5°, indicating its amorphous nature. Interestingly, the diffractograms of both Zn-NR and Zn-NR-GG nanoparticles did not exhibit specific peaks of NR. This suggests that NR was present in an amorphous state within the nanoparticles.[39] Furthermore, the diffractogram of the Zn-NR-GG nanoparticles differed significantly from that of the Zn-NR nanoparticles. The peaks observed in the diffractogram of the Zn-NR nanoparticles were notably reduced in intensity in the spectra of the Zn-NR-GG nanoparticles. This reduction suggests that the GG molecules effectively coated the Zn-NR nanoparticles.[6] Here, the reduction in peak intensity may be indicative of the successful establishment of a covering of GG around the Zn-NR nanoparticles. As well, it confirms the effective encapsulation of NR within the amorphous matrix of the Zn and GG.

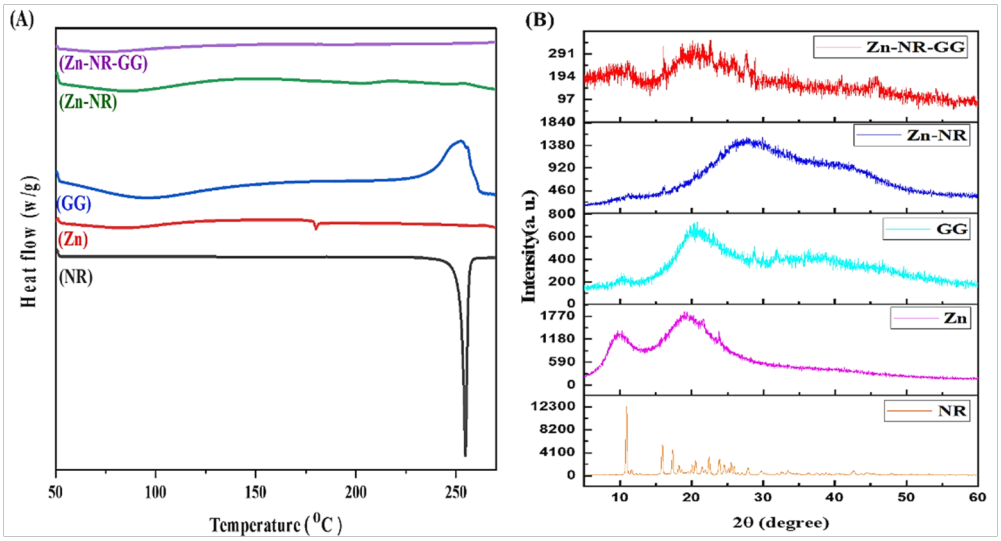

Figure 3: Thermograms (A) and diffractograms (B) of NR, Zn, GG, Zn-NR, and Zn-NR-GG nanoparticles

FTIR

Figure 4A displays the FTIR spectra of the NR and nanoparticles. The FTIR spectrum of NR shows characteristic peaks at 3104 cm^{-1}, 2913 cm^{-1}, 1155.26 cm^{-1}, and 1062.58 cm^{-1} corresponding to the stretching vibrations of O–H, asymmetric stretching vibrations of CH_2, C–O stretching, and C–O–C stretching vibrations, respectively.[40] In the case of the FTIR spectrum of GG, the peaks at 3244.0 cm^{-1}, 2915 cm^{-1}, 1597 cm^{-1}, 1396.32 cm^{-1}, and 1021 cm^{-1} indicated the stretching of –OH, −CH vibrations of the CH2 group, carboxylate anions (COO−), and the C–O stretch of carboxylic acids, respectively.[41,42] In the FTIR spectrum of Zn nanoparticles, the peaks at 3292.88 cm^{-1}, 1645.45 cm^{-1}, and 1532.0 cm^{-1} are associated with –OH groups, amide I groups (involving C–O stretching vibrations), and amide II groups (involving C–N stretching vibrations and N–H bending), respectively.[8,43] In the case of the FTIR spectrum of Zn-NR and Zn-NR-GG nanoparticles, the –OH peaks of Zn shifted to 3318 cm^{-1} and 3320 cm^{-1}, respectively, indicating the participation of hydrogen bonds in nanoparticle formation. In Zn-NR-GG nanoparticles, the amide I peak of Zn shifted from 1645 cm^{-1} to 1639 cm^{-1}, while in both Zn-NR and Zn-NR-GG nanoparticles, the amide II peak of Zn shifted to 1532 cm^{-1} and 1557.88 cm^{-1}, respectively. These shifts indicate the presence of electrostatic interactions during the formation of nanoparticles.[34]

Fluorescence spectroscopy

Fluorescence spectroscopy was employed to investigate the intermolecular interactions within the Zn, Zn-NR, and Zn-NR-GG nanoparticles (Fig. 4B). In all Zn based samples, the excitation peak was observed at 280 nm, and the emission peak was detected at 308 nm. This phenomenon is attributed to the presence of tyrosine and tryptophan residues in Zn, which are known to exhibit excitation at 280 nm.[44] The emission peaks of these groups are influenced by the local environment. Compared to pure Zn nanoparticles, the peak emission intensity noticeably decreased

in Zn-NR nanoparticles. This reduction can be attributed to NR's ability to quench the fluorescence emission of Zn through interactions such as hydrophobic and hydrogen bonding interactions.[6,45] Interestingly, the presence of GG as a shell, increased the fluorescence excitation of Zn. This was evidenced by the higher fluorescence intensity of the Zn-NR-GG nanoparticles than that of the Zn-NR nanoparticles. This enhancement may be attributed to structural changes in Zn induced by GG, which expose tryptophan residues that were previously shielded within the hydrophobic core.[46] Changes in protein conformation typically affect the fluorescence intensity of tryptophan residues.[47] Furthermore, the fluorescence intensity of Zn-NR-GG nanoparticles increased progressively with increasing GG concentration from 0.09 g to 1.8 g (ratios ranging from 10:1 to 1:1).[44]

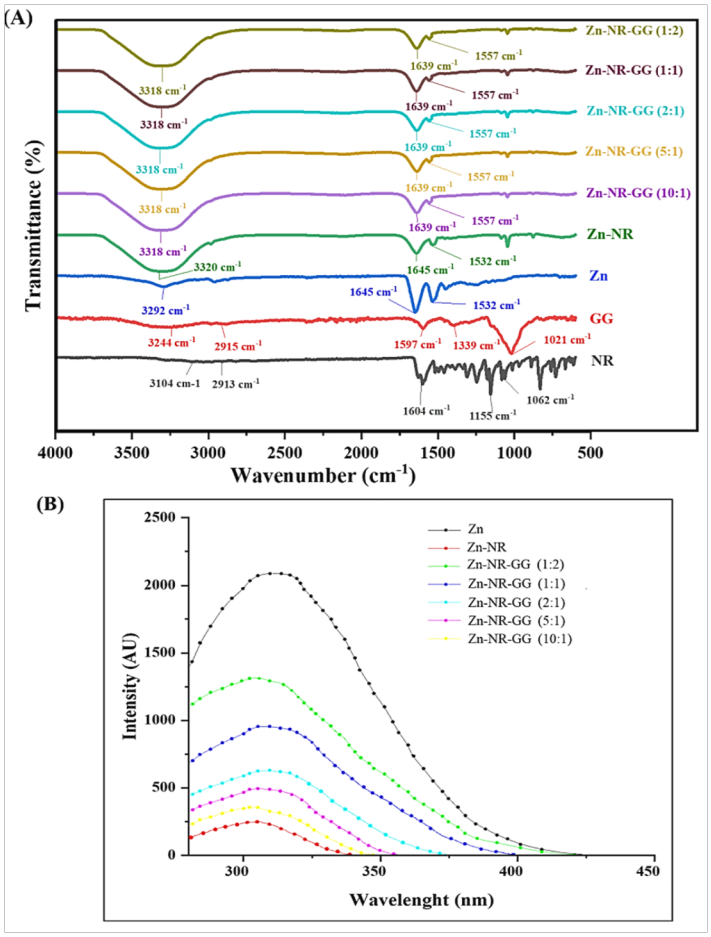

Figure 4: (A) FTIR spectra of NR, GG, Zn-NR and Zn-NR-GG nanoparticles; (B) Fluorescence spectra of Zn, Zn-NR, and Zn-NR-GG nanoparticles in deionized water

Stability evaluation

Thermal stability

As depicted in Figure 5A, the particle size of Zn-NR nanoparticles was found to be ranging from 161.5 ± 0.21 nm, 162.18 ± 0.46 nm, 165.02 ± 0.17 nm, 169.86 ± 0.38 nm, and 173.81 ± 0.16 nm to 175.02 ± 0.49 nm at temperatures ranging from 40 °C, 50 °C, 60 °C, 70 °C, 80 °C to 90 °C, respectively. Similarly, the particle size of Zn-NR-GG nanoparticles was found to be 234.13 ± 0.08 nm, 235.62 ± 0.29 nm, 237.45 ± 0.32 nm, 240.68 ± 0.09 nm, 243.07± 0.22 nm to 247.87 ± 0.08 nm with rising temperatures ranging from 40 °C, 50 °C, 60 °C, 70 °C, 80 °C to 90 °C, respectively. This indicates a constant nanoparticle size, which suggests a robust thermal stability of the prepared nanoparticles. Figure 5B shows minimal variations in zeta potential for Zn-NR-GG from -17.71 ± 0.26 mV to -16.92 ± 0.03 mV and Zn-NR from +12.48 ± 0.61 mV to +12.51 ± 0.6 mV. This confirms the good stability of the prepared nanoparticles at different temperatures. The hypothesized mechanism for this stability involves hydrogen bonding and hydrophobic

interactions within the Zn-NR-GG nanoparticles, which likely inhibit aggregation and enhance thermal stability during heating.[48] Overall, the designed Zn-NR-GG nanoparticles exhibited good thermal stability.

Ionic strength stability

In this study, the particle sizes of Zn-NR nanoparticles were found to be 160.14 ± 0.4 nm, 190.98 ± 0.41 nm, 530.02 ± 1.62 nm, 921.52 ± 3.36 nm, 1345.25 ± 0.61 nm, and 1306.40 ± 20 nm after addition of NaCl of 0 mM, 10 mM, 20 mM, 50 mM, 100 mM, and 200 mM, respectively. It showed sensitivity to salt concentration, as evidenced by the significant increase in particle size (Fig. 5C). Moreover, the results showed a decrease in zeta potential from 12.48 ± 0.04 mV to 3.6 ± 0.10 mV (Fig. 5D). This behavior was due to the interaction between the positively charged surface of the Zn nanoparticles and the anionic chloride ions from NaCl, which reduced the overall surface charge. This reduction in surface charge diminishes the electrostatic repulsion between the particles, making them more prone to aggregation. As the electrostatic repulsion weakens, the attractive forces between particles become more dominant, promoting aggregation.

In contrast, Zn-NR-GG nanoparticles exhibited remarkable stability under the same conditions. In brief, the particle size was found to be 235.19 ± 0.67 nm, 238.61 ± 0.49 nm, 239.55 ± 0.05 nm, 240.16 ± 0.09 nm, 241.2 ± 0.26 nm, and 241.27 ±15 nm after addition of NaCl of 0 mM, 10 mM, 20 mM, 50 mM, 100 mM, and 200 mM, respectively. Here, it resulted in a decrease in zeta potential from -17.71 ± 0.03 mV to -16.03 ± 0.05 mV (Fig. 5D). In addition, the particle size remained unchanged (Fig. 5C). This stability is attributed to the sustained electrostatic repulsion provided by the surface charges of the nanoparticles, which prevents aggregation.[2] The GG coating played a crucial role in this stability. It contributes to steric hindrance, creating a physical barrier that keeps particles from coming too close.

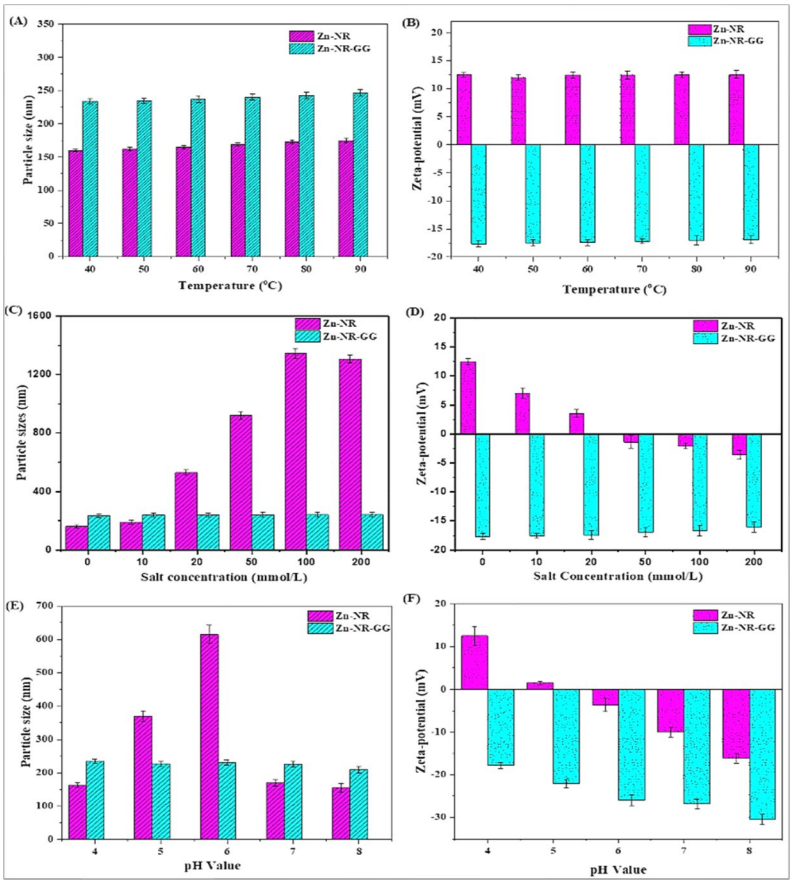

Figure 5: Thermal stability of Zn-NR and Zn-NR-GG: (A) Particle size and (B) Zeta potential; Ionic stability of Zn-NR and Zn-NR-GG: (C) Particle size, (D) Zeta-potential; pH stability of Zn-NR and Zn-NR-GG: (E) Particle size, (F) Zeta-potential

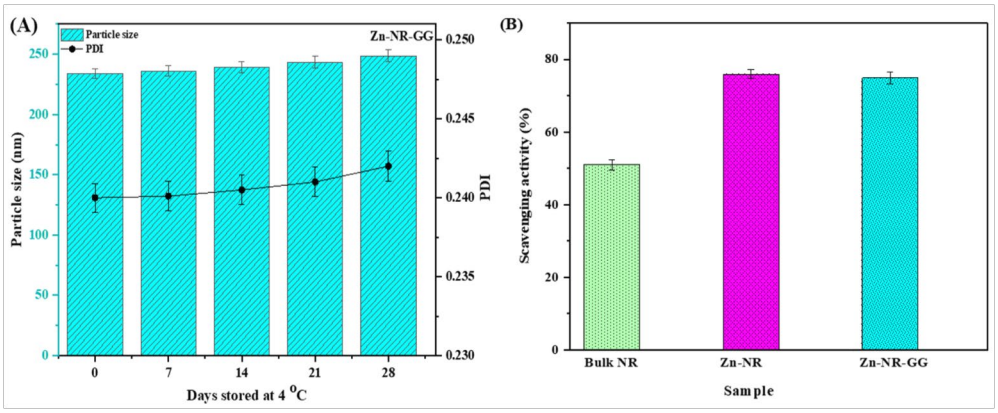

Figure 6: Storage stability (A) of Zn-NR-GG and antioxidant activity (B) of NR, Zn-NR, and Zn-NR-GG

This steric hindrance, combined with residual electrostatic repulsion, effectively prevents nanoparticle aggregation, even at high salt concentrations.[49]

pH Stability

In this study, Zn-NR-GG nanoparticles showed a progressive decrease in particle size from 234.1 ± 0.15 nm, to 227.47 ± 0.36 nm, 231.76 ± 0.46 nm, 225.30 ± 0.40 nm and 209.53 ± 0.21 nm as the pH increased from 4.0, to 5.0, 6.0, 7.0 and 8.0, respectively (Fig. 5E). This is due to the enhanced electrostatic repulsion and higher surface charges among the nanoparticles at higher pH values. The Zn-NR nanoparticles exhibited a relatively low zeta potential -3.7 ± 0.05 mV as they approached the Zn isoelectric point, which is around pH 6.0 (as shown in Fig. 5F). This led to significant aggregation due to weakened electrostatic repulsion. In contrast, at the same pH, the Zn-NR-GG nanoparticles did not undergo aggregation, indicating that the presence of GG gel effectively prevented Zn nanoparticle aggregation.

Storage stability

Particle size analysis of the Zn-NR-GG samples showed no major changes in the size of the particles, while the PDI exhibited no significant differences ($p > 0.05$) by day 28, as shown in Figure 6A. Here, the particle size was found to be 234.21 ± 0.02 nm, 236.21 ± 0.31 nm, 239.36 ±0.024 nm, 243.51 ± 0.46 nm, and 248.6 ± 0.39 nm on days 0, 7, 14, 21, and 28, respectively, at 4 °C. Here, the PDI increased slightly from 0.240 ± 0.11 to 0.242 ± 0.07. This demonstrates that the steric repulsion provided by the GG coating effectively prevented the aggregation of the Zn-NR-GG nanoparticles.

***In vitro* antioxidant activity**

The free radical scavenging potential of both free NR and NR encapsulated within nanoparticles was assessed using the DPPH free radical scavenging assay, as illustrated in Figure 6B. In brief, the Zn-NR nanoparticles exhibited a higher DPPH radical scavenging ability (71.2 ± 0.31%) than free NR (51.3 ± 0.05%). This indicates that encapsulating NR within Zn-NR nanoparticles is an effective strategy to enhance their antioxidant activity. The improvement in the antioxidant activity was likely due to the hydrophilic core-shell structure of the prepared nanoparticles. Encapsulated hydrophobic nutraceuticals offer enhanced dispersibility in aqueous solutions and improve the interaction between nutraceuticals and free radicals.[50,51] Additionally, the radical scavenging capacity of Zn-NR-GG nanoparticles did not significantly differ from that of Zn-NR nanoparticles when coated with GG and crosslinked with Ca^{2+}. This result suggests that the strategy to enhance the physicochemical stability of nutraceuticals does not compromise their functional characteristics.[52]

Simulated gastrointestinal digestion

Figure 7 shows the simulated gastrointestinal release of NR from the Zn, GG, and Zn-GG-based nanoparticles. In brief, NR-GG showed 50.39 ± 0.03% in 1 h at 1.2 pH and 85.17 ± 0.02% release of NR in 3 h at 7.4 pH. Similarly, Zn-NR showed 25.48 ± 0.24% in 1 h at 1.2 pH and 66.82 ± 0.24% in 3 h at 7.4 pH release of NR. The final prepared Zn-NR-GG (5:1) showed 19.60 ± 0.06% in 1 h at 1.2 pH and 59.99 ± 0.16% NR was released in 3 h

at 7.4. On the contrary, the NR release from deionized water was found to be 2.11 ± 0.018% in 1 h at 1.2 pH and 27.62 ± 0.43% in 3 h at 7.4 pH. Here, the NR release from deionized water was limited because of its low solubility in water, which restricted the release of NR in gastrointestinal fluid.[48] In brief, the NR present in the nanoparticles was consistently discharged during both the simulated gastric phase (0–60 min) and the small intestine phase (60–240 min). The discharge rate varied depending on the system.

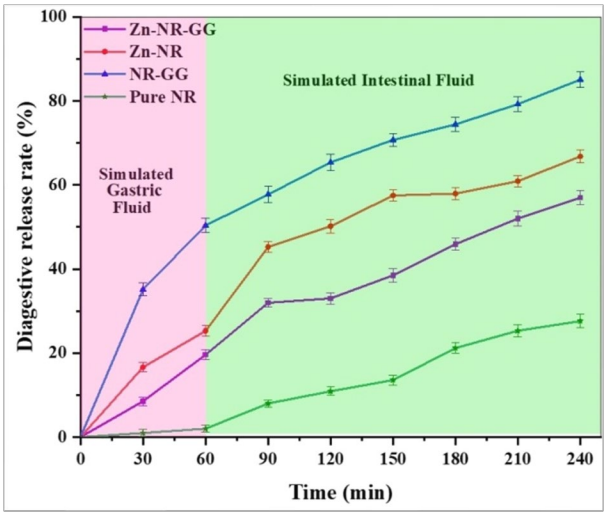

Figure 7: Simulated gastrointestinal digestion of NR in water, Zn-NR, NR-GG, and Zn-NR-GG

Table 1
Kinetic models for Zn-NR-GG

Kinetic models	Regression coefficient (R^2)
Zero-order	0.95 ± 0.05
First-order	0.99 ± 0.001
Higuchi	0.93 ± 0.70
Korsmeyer-Peppas	0.98 ± 0.13
Hixson-Crowell	0.98 ± 0.00

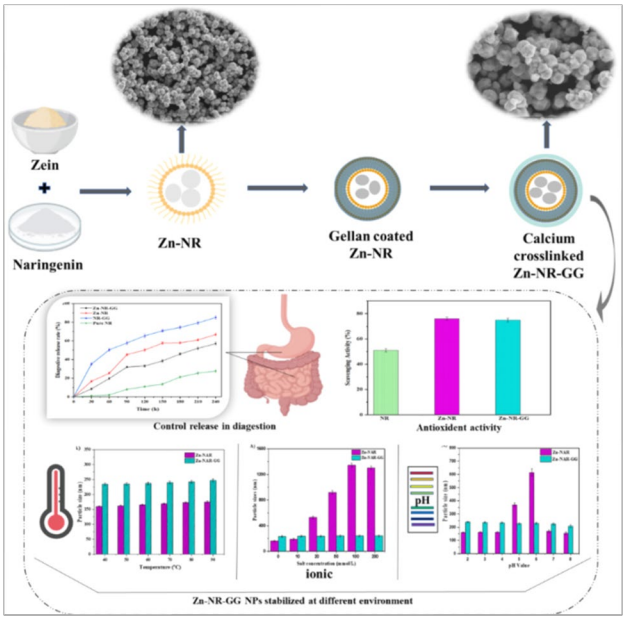

Figure 8: Formulation of calcium-crosslinked zein-gellan gum nanoparticles for naringenin delivery: stability, digestion simulation, and antioxidant evaluation

Notably, the NR release from Zn-NR-GG nanoparticles consistently showed lower levels compared to both the NR-GG and Zn-NR nanoparticles. This reduction could be attributed to the formation of Ca^{2+} ions with the GG coating on the Zn nanoparticles. It slows down the breakdown of the nanoparticles in the gastrointestinal environment, thereby reducing the rate of NR release. Table 1 summarizes the release kinetics of the developed Zn-NR-GG biopolymer nanoparticle. The first-order release kinetic model was found to be the best fit, with a regression coefficient (R^2) of 0.99 ± 0.008. Consequently, the obtained results suggest that Zn-NR-GG nanoparticles enhanced the NR stability in gastrointestinal conditions. In the future, there is a need to perform a premium study of the remaining formulations to ensure the bioavailability enhancement of NR.

CONCLUSION

The designed core-shell biopolymer nanoparticles consist of a hydrophilic shell (Ca^{2+} crosslinked GG) and a hydrophobic core (Zn), which offer sustained release of naringenin (NR) and improve the stability of Zn nanoparticles in GIT media. The prepared Zn-NR-GG nanoparticles exhibits good fluorescence properties due to high binding affinity between NR and Zn, nanoscale dimensions, and excellent stability in water. In these nanoparticles, NR and Zn interact through hydrophobic and hydrogen bonding, while Zn and GG exhibit electrostatic attraction. The GG coating on the surface of Zn-NR nanoparticles provides a smooth surface morphology and results in an increase in particle size compared to uncoated Zn-NR nanoparticles. The GG coating on NR-encapsulated Zn nanoparticles enhances their stability against heat, salts, pH variations, and storage conditions, potentially due to interactions maintained with nanoparticles. Additionally, the GG coating enhanced the antioxidant activity compared to the individual components of the nanoparticles, likely because of the hydrophilic core-shell structure of the prepared nanoparticles. Overall, the Zn-NR-GG design provides excellent entrapment efficiency, stability, improved antioxidant activity, and sustained release of NR. Therefore, future use of GG and Zn can further improve the stability and modulate the release of active compounds.

ACKNOWLEDGMENT: The authors extend their gratitude to the Management and Principal of the H. R. Patel Institute of Pharmaceutical Education and Research for providing the necessary facilities for the successful completion of this research.

REFERENCES

[1] C. Elizabeth, Master's Thesis, Graduate School New Brunswick Rutgers, the State University of New Jersey Rutgers, 2016, https://doi.org/doi:10.7282/T31N835G

[2] B. Duan, Y. Li, H. Geng, A. Ma and X. Yang, *Int. J. Clin. Pract.*, **75**, e14509 (2021), https://doi.org/10.1111/ijcp.14509

[3] T. Macedo, F. Pavia Martins, F. Ferreres, N. Gomes, A. Oliveira *et al*., *Bioorg. Chem*., **138**, 106614 (2023), https://doi.org/10.1016/j.bioorg.2023.106614

[4] M. Yıldırım, Ö. Acet, D. Yetkin, B. Acet, V. Karakoc *et al*., *J. Drug Deliv. Technol*., **74**, 103552 (2022), https://doi.org/10.1016/j.jddst.2022.103552

[5] V. Sarojamma and R. Vadde, *Onco Therap*., **9**, 25 (2022), https://doi.org/10.1615/OncoTherap.2022044893

[6] A. Dayarathne, S. Ranaweera, P. Natraj, P Rajan, K. Song *et al*., in *Procs. 2020 Kalas International Symposium*, 2020, https://doi.org/10.13140/RG.2.2.25037.67042

[7] S. Jiang, F. Ma, J. Lou, J. Li, X. Shang *et al*., *Eur. J. Pharmacol*., **970**, 176455 (2024), https://doi.org/10.1016/j.ejphar.2024.176455

[8] N. Zaidun, Z. Thent and A. Latiff, *Life Sci*., **208**, 111 (2018), https://doi.org/10.1016/j.lfs.2018.07.017

[9] G. Zhang, H. Guan, J. Li, M. Li, X. Sui *et al*., *Asian J. Pharm. Sci*., **17**, 741 (2022), https://doi.org/10.1016/j.ajps.2022.09.001

[10] N. Nasri, B. Uddin, Z. Sarkar, C. Ling, L. Bin *et al*., *J. Pharm. Negat. Results*, **13**, 104 (2022), 0.47750/pnr.2022.13.S07.016

[11] M. Marwah, R. Badhan and D. Lowry, *J. Liposome Res*., **32**, 181 (2022), https://doi.org/10.1080/08982104.2021.1956529

[12] J. Jacob, J. Haponuik, S. Thomas and S. Gopi, *Mater. Today Chem*., **9**, 43 (2018), https://doi.org/10.1016/j.mtchem.2018.05.002

[13] Z. Zhang, X. Li, S. Sang, D. J. McClements, L. Chen *et al*., *Food Chem*., **403**, 134344 (2023), https://doi.org/10.1016/j.foodchem.2022.134344

[14] Y. Yuan, H. Li, C. Liu, J. Zhu, Y. Xu *et al*., *Int. J. Biol. Macromol*., **139**, 30 (2019), https://doi.org/10.1016/j.ijbiomac.2019.07.090

[15] C. J. Cheng and O. G. Jones, *Food Hydrocoll*., **69**, 28 (2017), https://doi.org/10.1016/j.foodhyd.2017.01.022

[16] H. Li, D. Wang, C. Liu, J. Zhu, M. Fan *et al*., *Food Hydrocoll*., **87**, 342 (2019), https://doi.org/10.1016/j.foodhyd.2018.08.002

[17] J. Liu, Y. Li, H. Zhang, S. Liu, M. Yang *et al*., *Food Chem*., **372**, 131266 (2022), https://doi.org/10.1016/j.foodchem.2021.131266
[18] R. Meng, Z. Wu, Q. T. Xie, J. S. Cheng and B. Zhang, *Food Chem*., **340**, 127893 (2021), https://doi.org/10.1016/j.foodchem.2020.127893
[19] J. Yang, J. Lin, X. Chen, L. Rang, M. Shen *et al*., *Carbohyd. Polym*., **295**, 119875 (2022), https://doi.org/10.1016/j.carbpol.2022.119875
[20] R. Ding, M. Zhang, Q. Zhu, Y. Qu, X. Jia *et al*., *Int. J. Biol. Macromol*., **251**, 126201 (2023), https://doi.org/10.1016/j.ijbiomac.2023.126201
[21] P. E. Jansson, B. Lindberg and P. A. Stanford, *Carbohyd. Res*., **124**, 135 (1983), https://doi.org/10.1016/0008-6215(83)88361-X
[22] J. T. Oliveira, T. C. Santos, L. Martins, R. Picciochi, A. P. Marques *et al*., *Tissue Eng. Part A*, **16**, 343 (2010), https://doi.org/10.1089/ten.TEA.2009.0117
[23] L. Fasolin, C. Picone, R. Santana and R. Cunha, *Food Res. Int*., **54**, 501 (2013), https://doi.org/10.1016/j.foodres.2013.07.026
[24] H. Warren and M. Panhuis, *Synth. Met*., **206**, 61 (2015), https://doi.org/10.1016/j.synthmet.2015.05.004
[25] X. Zhang, D. Liu, T. Jin, W. Chen, Q. He *et al*., *Food Hydrocoll*., **114**, 106570 (2021), https://doi.org/10.1016/j.foodhyd.2020.106570
[26] J. Vilela and R. Cunha, *Food Res. Int*., **91**, 47 (2017), https://doi.org/10.1016/j.foodres.2016.11.020
[27] K. Hu, X. Huang, Y. Gao, X. Huang, H. Xiao *et al*., *Food Chem*., **182**, 275 (2015), https://doi.org/10.1016/j.foodchem.2015.03.009
[28] P. Shinde, H. Agrawal, A. Singh, U. Yadav and U. Kumar, *J. Drug Deliv. Sci. Technol*., **52**, 369 (2019), https://doi.org/10.1016/j.jddst.2019.04.044
[29] H. Xie, C. Liu, J. Gao, J. Shi, F. Ni *et al*., *Food Chem*., **365**, 130542 (2021), https://doi.org/10.1016/j.foodchem.2021.130542
[30] Q. Ge, S. Rang, C. Yin, D. McClements, Q. Fu *et al*., *Food Chem*., **434**, 137488 (2024), https://doi.org/10.1016/j.foodchem.2023.137488
[31] Y. Yin, T. Jiang, Y. Hao, J. Zhang, W. Li *et al*., *Int. J. Pharm*., **606**, 120937 (2021), https://doi.org/10.1016/j.ijpharm.2021.120937
[32] S. Chen, Y. Ma, L. Dai, W. Liao, J. Liu *et al*., *Food Hydrocoll*., **118**, 106758 (2021), https://doi.org/10.1016/j.foodhyd.2021.106758
[33] Y. Luo and Q. Wang, *J. Appl. Polym. Sci*., **131**, 40696 (2014), https://doi.org/10.1002/app.40696
[34] N. Oghaz, A. Asoodeh and M. Mohammadi, *Int. J. Biol. Macromol*., **204**, 576 (2022), https://doi.org/10.1016/j.ijbiomac.2022.02.041
[35] X. Li, P. Zhou, Z. Luo, R. Feng and L. Wang, *Int. J. Biol. Macromol*., **203**, 244 (2022), https://doi.org/10.1016/j.ijbiomac.2022.01.143
[36] C. Sun, Y. Wei, R. Li, L. Dai and Y. Gao, *J. Agric. Food Chem*., **65**, 3934 (2017), https://doi.org/10.1021/acs.jafc.7b00921
[37] G. Zhang, G. Sun, H. Guan, M. Li, Y. Liu *et al*., *Asian J. Pharm. Sci*., **16**, 816 (2021), https://doi.org/10.1016/j.ajps.2021.09.001
[38] I. Nallamuthu, V. Ponnusamy, M. Smruthi and F. Khanun, *J. Clust. Sci*., **32**, 1649 (2021), https://doi.org/10.1007/s10876-020-01909-1
[39] S. Jiang, F. Ma, J. Luo, J. Li, Y. Li *et al*., *Eur. J. Pharmacol*., **970**, 176455 (2024), https://doi.org/10.1016/j.ejphar.2024.176455
[40] P. Ji, T. Yu, Y. Liu, J. Giang, J. Xu *et al*., *Drug Des. Dev. Ther*., **10**, 911 (2016), https://doi.org/10.2147/DDDT.S97738
[41] V. Cardoso, N. Brito, N. Ferreira, F. Boni, L. Ferreira *et al*., *Colloids Surf. A*: *Physicochem. Eng. Asp*., **628**, 127321 (2021), https://doi.org/10.1016/j.colsurfa.2021.127321
[42] A. Jaafar and V. Thatchinamoorthi, *IOP Conf. Ser.*: *Mater. Sci. Eng*. **440**, 012023 (2018), https://doi.org/10.1088/1757-899X/440/1/012023
[43] T. Wu, W. Han, Y. Han, L. Ma, M. Li *et al*., *J. Mol. Liq*., **386**, 122569 (2023), https://doi.org/10.1016/j.molliq.2023.122569
[44] Q. Liu, J. Chen, Y. Qin, B. Jiang and T. Zhang, *Int. J. Biol. Macromol*., **158**, 461 (2020), https://doi.org/10.1016/j.ijbiomac.2020.04.128
[45] A. Moeiniafshari, A. Zarrabi and A. Bordbar, *Food Hydrocoll*., **51**, 1 (2015), https://doi.org/10.1016/j.foodhyd.2015.04.036
[46] X. Ren, T. Hou, Q. Liang, X. Zhang, D. Hu *et al*., *Food Chem*., **279**, 223 (2019), https://doi.org/10.1016/j.foodchem.2018.11.025
[47] H. Li, Y. Yuan, J. Zhu, T. Wang, D. Wang *et al*., *Food Hydrocoll*., **103**, 105715 (2020), https://doi.org/10.1016/j.foodhyd.2020.105715
[48] G. Ye, T. Wu, Z. Li, M. Teng, L. Ma *et al*., *Food Chem*., **417**, 135890 (2023), https://doi.org/10.1016/j.foodchem.2023.135890
[49] K. Hu and D. McClements, *Food Hydrocoll*., **44**, 101 (2015), https://doi.org/10.1016/j.foodhyd.2014.09.015
[50] X. Wang, M. Li, F. Liu, F. Peng, F. Li *et al*., *Food Chem*., **364**, 130335 (2021), https://doi.org/10.1016/j.foodchem.2021.130335
[51] X. Huang, X. Huang, Y. Gong, H. Xiao, D. McClements *et al*., *Food Res. Int*., **87**, 1 (2016), https://doi.org/10.1016/j.foodres.2016.06.009
[52] S. Chen, Q. Li, D. McClements, Y. Han, L. Dai *et al*., *Food Hydrocoll*., **99**, 105334 (2020), https://doi.org/10.1016/j.foodhyd.2019.105334